THE JOURNAL OF PHYSICAL CHEMISTRY C

Article

Cite This: J. Phys. Chem. C 2018, 122, 22024−22032

pubs.acs.org/JPCC

# Ethanol Decomposition on Pd−Au Alloy Catalysts

Hao Li,[†,§] Edward J. Evans, Jr.,[‡,§] C. Buddie Mullins,*[,‡] and Graeme Henkelman*[,†]

[†]Department of Chemistry and the Institute for Computational Engineering and Sciences, The University of Texas at Austin, 105 East 24th Street, Stop A5300, Austin, Texas 78712, United States

[‡]McKetta Department of Chemical Engineering and Department of Chemistry, Texas Materials Institute, Center for Electrochemistry, University of Texas at Austin, Austin, Texas 78712, United States

Supporting Information

**ABSTRACT:** The mechanisms of ethanol (EtOH) decomposition via C−C or C−O bond cleavage on alloy surfaces are currently not well understood. In this study, we model EtOH decomposition on close-packed Pd−Au catalytic surfaces using density functional theory (DFT) calculations and derived Brønsted−Evans−Polanyi (BEP) relationships. Three characteristic Pd−Au surfaces are considered, $Pd_1Au_2(111)$, $Pd_2Au_1(111)$, and a Pd monolayer (ML), $Pd_{ML}(111)$, on a Au substrate. We show that, on close-packed Pd−Au surfaces, the C−C bond is easier to cleave than C−O, indicating that the formation of $CH_4$ and CO is favored as the products of EtOH decomposition. Interestingly, we find that, though the C−C and C−O activation barriers on $Pd_{ML}(111)$ are generally lower than those on the other two surfaces, it is less active for EtOH decomposition due to a slow release of $H_2$ and possible carbon coking. $Pd_2Au_1(111)$, on the other hand, has a higher theoretical reaction rate due to facile $H_2$ evolution from the surface and less carbon coking. A comparison of the surface d-band with the activation energy barriers shows that there is a trade-off between the barriers for C−C bond cleavage and $H_2$ association, with $Pd_2Au_1(111)$ having the best performance. Temperature-programmed desorption experiments of EtOH on Pd/Au surfaces show significant C−C bond cleavage and both $CH_4$ and CO production on surfaces with Pd−Au interface sites. Furthermore, neither Auger electron spectroscopy nor EtOH reflection−adsorption infrared spectroscopy provide evidence of C−O bond cleavage. Finally, the experimental reaction rate for methane production from C−C bond cleavage was higher on surfaces with more Au present due to minimal carbon contamination and the promotion of product desorption. This combined theoretical and experimental study shows that, though Au is catalytically inactive for EtOH decomposition, it can dramatically promote the surface activity for EtOH steam reforming due to the existence of active Pd−Au surface ensemble sites.

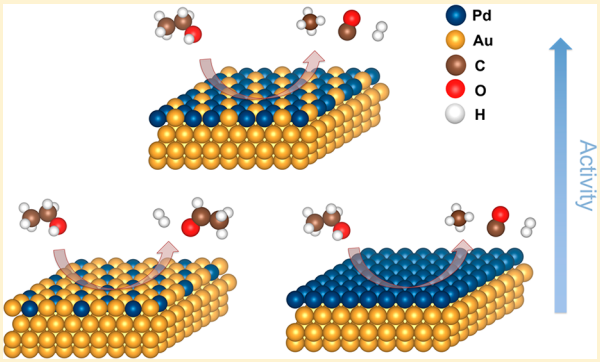


## 1. INTRODUCTION

Alloy catalysts are important because of their capacity for tuning adsorbate binding energies and catalytic activity.[1,2] Many alloy catalysts have shown promising activity and/or selectivity for industrially significant heterogeneous catalysis, such as oxygen reduction,[3,4] hydrogen evolution,[2,5] CO oxidation,[2,6] hydrogenation,[1,7−9] and dehydrogenation.[10−12] Understanding catalytic mechanisms on alloy surfaces can be difficult for two reasons: (i) there are several effects, including strain, electronic, and atomic ensembles,[13] that affect activity; (ii) experimental determination of short-lived intermediates or transition states is difficult. Therefore, the rational design and tailoring of alloyed catalytic surfaces for specific reactions is particularly challenging but also very important.

Ethanol (EtOH) decomposition is a key step in industrially relevant reactions such as EtOH steam reforming and EtOH partial oxidation, whether as an unwanted side reaction or a step in the desired reaction.[14] Compared to simpler reactions, EtOH decomposition is less well understood due to the numerous possible dehydrogenation steps as well as the possible order of C−C and C−O bond cleavage on various surfaces.[10,12,15−17] To understand the EtOH decomposition mechanism, density functional theory (DFT) has proven to be a powerful method for monometallic surface studies including Pd,[18] Pt,[19] and Rh.[20,21] Using DFT and Brønsted−Evans−Polanyi (BEP) relationships, Dumesic et al.[16] developed a model for specific C−C and C−O bond cleavage for EtOH species on Pt(111), with good agreement with experiments.[22] Mavrikakis et al.[17] further generalized this method with scaling relationships that allowed for modeling EtOH decomposition on the close-packed surfaces of Cu, Pt, Pd, Ni, Ir, Rh, Co, Os, Ru, and Re. Their combined modeling and experimental study showed that most of these transition metals favor C−C bond cleavage of the CHCO species, leading to the selective formation of $CH_4$. Weststrate et al.[23] then experimentally found that C−O cleavage is also feasible on Co(0001), suggesting that there are still mysteries related to EtOH

Received: August 21, 2018
Published: August 30, 2018







DOI: 10.1021/acs.jpcc.8b08150
J. Phys. Chem. C 2018, 122, 22024−22032

decomposition on catalysts. Xu et al.[24,25] also systematically studied the $Pt_3M$ (M = Pt, Ru, Sn, Re, Rh, and Pd) catalysts for EtOH partial oxidation with DFT calculations. Very recently, we found that different surface ensembles of PdAu(111) and RhAu(111) lead to a variety of EtOH dehydrogenation activities and selectivities.[10,12] Specifically, it was shown that tailoring the specific alloy ensembles could selectively target specific initial dehydrogenation of O−H, $\alpha$-C−H, or $\beta$-C−H.[10] Experimentally, Kumar et al.[26] found that, similar to Ni, EtOH decomposition on CuNi bimetallic alloys leads to C−C bond cleavage, while pure Cu leads to only acetaldehyde at low temperature. Skoplyak et al.[27] found that M/Pt(111) (M = Ni, Fe, and Ti) bimetallic surfaces yield high $H_2$ production during EtOH reforming, with trends that correlate well with the calculated d-band center. However, due to the variety of dehydrogenated EtOH species and computational cost of many activation energy calculations, to the best of our knowledge, a kinetic and thermodynamic understanding of EtOH decomposition on an alloyed surface is not yet established.

As a miscible bimetallic, PdAu alloy is widely studied as a catalyst because it is relatively easy to prepare, it has good tunability of adsorbate binding, and it shows versatile catalytic performance.[1,11,12,28−30] Our previous studies have found that, though Au is catalytically inactive for hydrogenation/dehydrogenation, the addition of Pd onto Au surfaces can result in enhanced alkane and allyl alcohol hydrogenation as compared to monometallic Pd.[1,9] Our recent study on PdAu close-packed surfaces shows that a very small amount of Pd alloyed on Au(111) leads to the selective formation of $H_2$ and acetaldehyde, while, when the surface contains predominately Pd−Au interface sites, there is a high production of $H_2$ and CO.[12] Motivated by this result and the recognition that the mechanism of EtOH decomposition can affect the products of EtOH reactions, we selected a PdAu(111) alloy catalyst as a case study for modeling EtOH decomposition. Using DFT calculations, we found that, on PdAu(111) surfaces, C−C bond cleavage is favorable, leading to selective $CH_4$ and CO formation. Our model shows that Pd(111)-like sites are favorable for C−C bond cleavage but can also result in coking, while Pd−Au interface sites are more favorable for $H_2$ desorption and resist coking. To support our model, ultrahigh vacuum (UHV) experiments were performed on two Pd−Au catalysts with different surface site compositions, to show the production of $CH_4$, CO, and carbon poisoning, in good agreement with our theoretical predictions.

## 2. METHODS

**2.1. Computational and Modeling Methods.** All DFT calculations were performed using the Vienna *ab initio* simulation package (VASP). A projector augmented-wave method was used to describe the core electrons.[31] The generalized gradient approximation with the Perdew−Burke−Ernzerhof (PBE) functional was employed to describe the electronic exchange and electronic correlation.[32] For the valence electrons, Kohn−Sham wave functions were expanded in a plane wave basis.[33] The energy cutoff of all calculations was set at 300 eV. Soft potentials were used to describe the electrons of oxygen and carbon. The Brillouin zone was sampled with a 3 × 3 × 1 Monkhorst−Pack *k*-point mesh. Geometries were optimized when the force per atom was lower than 0.05 eV/Å. All transition states and energy barriers were calculated using the climbing image nudged elastic band (ClNEB) method,[34] where more than five intermediate images were generated between the initial and final states. Convergence tests were performed by increasing the cutoff, force criterion, and number of layers in the slab model, with standard PAW potentials (Tables S1 and S2); no significant changes in the binding energies, energy barriers, or the optimized structures were found. Spin-polarization was tested and found to have a negligible influence on the thermodynamic and kinetic results. Therefore, spin polarization was not included in the calculated results of this paper.

In regard to influencing the selectivity and activity for hydrogenation, dehydrogenation, and oxygen reduction reaction on alloy surfaces, our previous studies show that atomic ensemble effects are generally more significant as compared to electronic (ligand) and strain effects when considering the adsorption of hydrogen, oxygen, hydroxyl, and other EtOH-related species.[7−10,12,28] This observation is consistent with our current results showing similar binding energies on Pd monolayers (MLs) on different subsurface alloys, while the binding energies on three surfaces with different surface compositions, shown in Figure 1, are

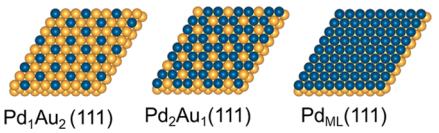


**Figure 1.** Three types of PdAu(111) surfaces considered in our DFT calculations, consisting of the triatomic ensembles of $Pd_1Au_2$, $Pd_2Au_1$, and $Pd_3$. Blue and golden spheres represent Pd and Au atoms, respectively.

significantly different (Table S3). This shows that the contributions from subsurface alloying and surface strain to the binding energy of adsorbates are less important than the ensemble effect for our random alloys. Therefore, we do not consider the sublayer composition in our study. On the PdAu(111) alloy surfaces, the triatomic ensembles ($Au_3$, $Pd_1Au_2$, $Pd_2Au_1$, and $Pd_3$) are the smallest unit that determine adsorbate binding of H, O, OH, and CO.[1,9,13,28] In light of this result, all calculations were performed on the three PdAu surfaces: $Pd_1Au_2$(111), $Pd_2Au_1$(111), and $Pd_{ML}$(111) shown in Figure 1; these surfaces present the $Pd_1Au_2$, $Pd_2Au_1$, and $Pd_3$ triatomic ensembles, respectively. Previous theoretical studies show that these three alloy surfaces are representative models for the evaluation of ensemble effects on close-packed surfaces.[29,35] All three surfaces were modeled as a four-layer slab with (3 × 3) unit cells, with a vacuum layer of 12 Å separating periodic images of the slab. For each slab, the bottom two atomic layers were kept fixed in bulk positions, while the topmost two layers were allowed to relax freely. The lattice constant *C* used for this study was calculated according to the composition of Pd−Au in the model

$$C = C_{Pd}\cdot Pd\% + C_{Au}\cdot Au\% \quad (1)$$

where $C_{Pd}$ and $C_{Au}$ represent the lattice constants of Pd and Au, respectively, and Pd% and Au% represent the composition of Pd and Au, respectively. In this study, $C_{Pd}$ = 3.89 Å and $C_{Au}$ = 4.08 Å. Therefore, the lattice constants of $Pd_1Au_2$(111), $Pd_2Au_1$(111), and $Pd_{ML}$(111) are 4.06, 4.05, and 4.03 Å, respectively. All of the binding energies $E_b$ were calculated using eq 2


DOI: 10.1021/acs.jpcc.8b08150
J. Phys. Chem. C 2018, 122, 22024−22032

$$E_b = E_{ads*} - E_* - E_{ads} \quad (2)$$

where $E_{ads*}$ is the energy of the surface with adsorbate, $E_*$ is the energy of the bare surface, and $E_{ads}$ is the energy of the adsorbate in a vacuum.

**2.2. Experimental Methods.** In this study, experiments were performed in a molecular beam scattering UHV apparatus with a base pressure of $1 \times 10^{-10}$ Torr that has been described previously.[36,37] The apparatus is equipped with a quadrupole mass spectrometer (QMS) for detection of gaseous reactants and products, Auger electron spectroscopy (AES) with an electron beam energy of 3 keV and emission current of 1.5 mA to verify Pd deposition and cleanliness of the Au(111) substrate, and reflection−adsorption infrared spectroscopy with all spectra reported being an average of 512 scans at a resolution of 4 $cm^{-1}$.

The Pd−Au model catalysts were prepared by depositing Pd via a thermal evaporator onto a 11 mm diameter Au(111) single crystal surface at 77 K, followed by annealing at 500 K for 10 min. A quartz crystal microbalance controller was used to calibrate the Pd deposition rate with the assumption that the thickness of 1 Pd monolayer (ML) is equivalent to the diameter of a Pd atom (0.274 nm). Before Pd deposition, the Au(111) substrate was cleaned by argon ion bombardment (2 keV), followed by annealing to 800 K for 15 min. EtOH was exposed to our catalysts via a molecular beam that is defined by a series of aligned apertures. After exposure, temperature-programmed desorption (TPD) measurements were conducted by heating the Pd−Au catalysts at a rate of 1 K/s. Reactants and various potential products were monitored using their corresponding QMS signals.

## 3. RESULTS AND DISCUSSION

**3.1. C−C and C−O Cleavage.** With the ClNEB method, we calculated the activation energies of C−C and C−O bond cleavage of EtOH and dehydrogenated EtOH species. In total, we calculated 34, 38, and 33 activation energies on the $Pd_1Au_2(111)$, $Pd_2Au_1(111)$, and $Pd_{ML}(111)$ surfaces, respectively. To estimate the remaining possible activation energy barriers, given all possible surface sites and bonds to cleave, a BEP relationship for each surface was acquired (Figure 2) using the transition state and final state energies ($E_{TS}$ and $E_{FS}$). It can be seen that the $R^2$ values of the three BEP relationships are high (0.94, 0.91, and 0.87, respectively), which justifies our use of linear scaling relationships. The slopes and intercepts of the three regression lines are similar. Reassuringly, these regression lines are also similar to a previous study on Pt(111) and Ru(0001),[17] which indicates that the BEP relationships of EtOH decomposition are fairly general on different close-packed surfaces.

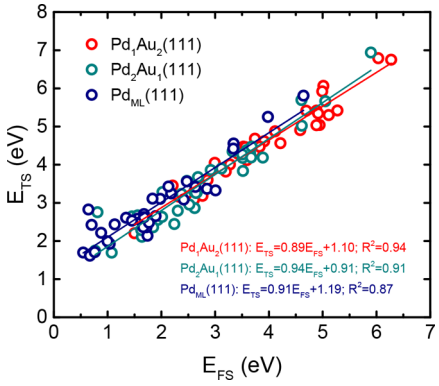


**Figure 2.** BEP correlation between the transition state (TS) energy and the final state (FS) energy for C−C and C−O bond cleavage on $Pd_1Au_2(111)$ (red), $Pd_2Au_1(111)$ (green), and $Pd_{ML}(111)$ (blue). The values of $E_{TS}$ and $E_{FS}$ are relative to the bare slab, EtOH (in gas phase) and $H_2$ (in gas phase).

Though activation energies can be acquired from the ClNEB method with DFT, there are still 39 missing activation energies due to the combinatorial complexity of the potential energy surfaces. Here, following a method similar to previous studies,[16,17] we use the BEP relationships acquired from Figure 2 to predict the activation energies of the remaining 39 C−C/C−O bond cleavage steps. To reduce the uncertainty in the model, we calculated all of the final state energies, $E_{FS}$, with DFT. All of the activation energy barriers (both calculated and BEP-predicted) are shown in Figure 3. It can be seen that, with a higher surface Pd composition, the energy barrier for both C−C and C−O bond cleavage generally decreases, in good agreement with our previous experimental and theoretical work.[10,12] This also shows that less dehydrogenated EtOH species tend to have a lower C−O bond cleavage barrier, while higher dehydrogenated EtOH species generally tend to have a lower C−C bond cleavage barrier.

To better understand C−C and C−O bond cleavage trends on the three surfaces, the projected density of states (PDOS) of the surface d-band were calculated and shown in Figure 4. It can be seen that, with increased Pd alloyed on the (111) surface, the PDOS is more contracted. Also, the d-band is closer to the Fermi level with more surface Pd, indicating more facile O−H, C−H, C−C, and C−O bond activation.[38] However, this upward shift of the d-band also leads to stronger binding of H and a possible bottleneck of $H_2$ evolution from the surface for EtOH decomposition. We will discuss these two effects in the following sections.

**3.2. Calculations of the Catalytic Activity for EtOH Decomposition.** The $H_2$ association barriers and cleavage of the C−O and C−C bonds, as presented in Table 1, show that the $H_2$ association energy generally increases with an increase of Pd composition, as we have seen previously.[12] In terms of the C−C and C−O bond cleavage, all steps are endothermic on $Pd_1Au_2(111)$, indicating a low EtOH decomposition activity, which is consistent with our previous experimental results: when the PdAu(111) surface contained a small amount of Pd, only acetaldehyde was detected during EtOH reforming and no subsequent products were detected.[12] On $Pd_2Au_1(111)$, all C−O bond cleavage steps are endothermic and only the C−C bond cleavage on CHCO is significantly exothermic (−0.48 eV). On $Pd_{ML}(111)$, $CH_2CH_2O$ has the only significant exothermic step for C−O bond breaking (−0.14 eV), while CHCO has the most exothermic C−C bond cleavage step (−0.89 eV). However, on $Pd_{ML}(111)$, C−O bond cleavage has a higher energy barrier (0.89 eV) than C−C bond cleavage (0.42 eV), indicating that C−C bond cleavage is the favorable step on $Pd_{ML}(111)$. Both for this reason and considering our subsequent experimental observation that no $C_2$ products were detected, we do not consider C−O bond cleavage in our kinetic model; additionally, our experiments, discussed later, justify this exclusion. The complete thermodynamic and kinetic data can be found in Tables S4 and S5. Interestingly, being similar to other close-packed transition metals,[17] CHCO has the most exothermic C−C bond cleavage steps on $Pd_2Au_1(111)$ and $Pd_{ML}(111)$ in our study. Although


DOI: 10.1021/acs.jpcc.8b08150
J. Phys. Chem. C 2018, 122, 22024−22032

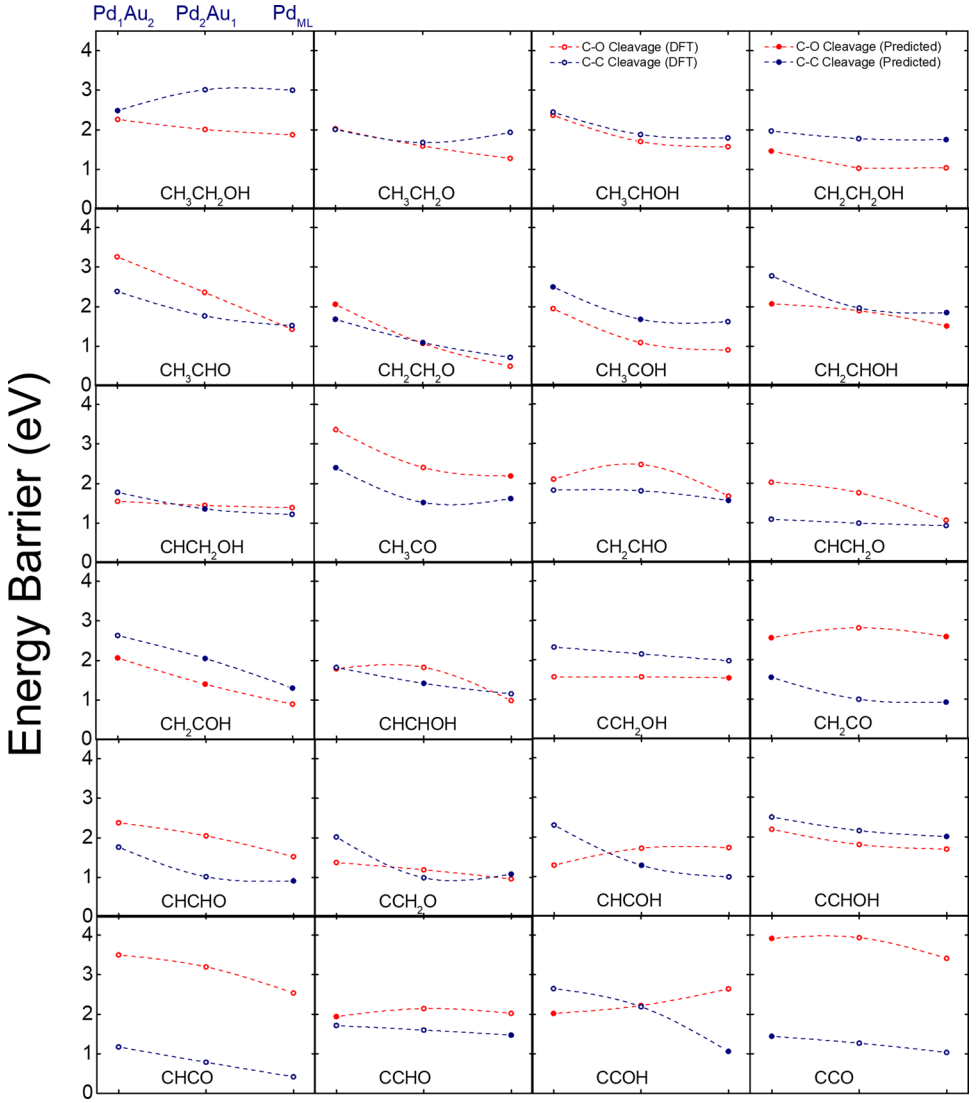


**Figure 3.** Activation energy barriers of the C−C (blue) and C−O (red) bond cleavage reactions. The empty circles were calculated with the ClNEB method. The solid circles were acquired from the BEP relationships shown in Figure 2.

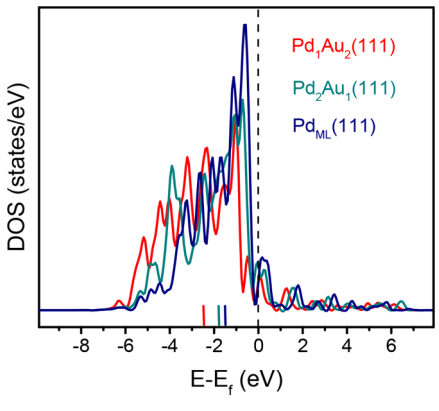


**Figure 4.** Projected density of states (PDOS) of the d-band of the surfaces of $Pd_1Au_2(111)$, $Pd_2Au_1(111)$, and $Pd_{ML}(111)$. The *x*-axis represents the energy relative to the Fermi energy level. The colored horizontal bars indicate the d-band centers of each distribution. The horizontal dashed line indicates the Fermi energy level.

there are also several intermediate species with exothermic steps found on $Pd_2Au_1(111)$ and $Pd_{ML}(111)$, CHCO still has the most significantly exothermic energy for C−C cleavage. Details of the reaction pathways at CHCO* can be found in Figure S1.

**Table 1. Energy and Chemical Information of C−O and C−C Bond Cleavage on the Three PdAu(111) Surfaces**

| | $Pd_1Au_2(111)$ | $Pd_2Au_1(111)$ | $Pd_{ML}(111)$ |
|---|---|---|---|
| $H_2$ association barrier (eV) | 0.43 | 0.61 | 1.13 |
| C−O cleavage species | *a* | *a* | $CH_2CH_2O$ |
| C−O cleavage reaction energy (eV) | all endothermic | all endothermic | −0.14 |
| C−O cleavage barrier (eV) | *a* | *a* | 0.89 |
| C−C cleavage species | all endothermic | CHCO | CHCO |
| C−C cleavage reaction energy (eV) | all endothermic | −0.48 | −0.89 |
| C−C cleavage barrier (eV) | *a* | 0.78 | 0.42 |

[a]The bond cleavage step of the corresponding EtOH-dehydrogenated species is not thermodynamically favorable. The complete data can be found in Table S4.

To model the reaction rates of C−C and C−O cleavage on PdAu(111), we used the simplified EtOH decomposition



DOI: 10.1021/acs.jpcc.8b08150
J. Phys. Chem. C 2018, 122, 22024−22032

kinetic model developed by Dumesic et al.,[16] with the assumption that, compared to C−C and C−O bond cleavage, the hydrogenation/dehydrogenation are in quasi equilibrium.[16,17,22] Afterward, the rates of C−C and C−O bond cleavages are considered to be controlled by

$$CH_3CH_2OH(g) + * \rightleftharpoons [CH_xCH_yOH_z*]^{\neq} + (6 - x - y - z)/2H_2(g) \quad (3)$$

where $x$, $y$, and $z$ represent the number of H atoms in their corresponding functional groups after EtOH dehydrogenation. From Table 1, we can see that the most favorable species for C−C bond cleavage is CHCO. Therefore, the rate of the C−C cleavage steps can be expressed in the combined step as follows:

$$CH_3CH_2OH(g) + * \rightleftharpoons [CHCO*]^{\neq} + 5/2H_2(g) \quad (4)$$

Then, according to the model developed by Dumesic et al.,[16] the rates of C−C bond cleavage on metallic surfaces can be derived from transition state theory (see the Supporting Information) and the theoretical activity of the C−C bond cleavage reaction rate $\log(r_{C-C})$ on $Pd_2Au_1(111)$ and $Pd_{ML}(111)$ can be calculated as a function of temperature (Figure 5). Although the C−C bond cleavage step on $Pd_2Au_1(111)$ has a higher energy barrier than that on $Pd_{ML}(111)$ (Table 1), its theoretical reaction rate is significantly higher than that of $Pd_{ML}(111)$. This is because $Pd_{ML}(111)$ has a higher $H_2$ desorption energy (1.21 eV) than $Pd_2Au_1(111)$ (0.68 eV), which leads to slower $H_2$ release from the $Pd_{ML}(111)$ surface, hindering subsequent C−C bond cleavage. The energy profile of $H_2$ desorption can be found in Figure S2. It should be noted that, in our experiments, if the PdAu alloy is randomly distributed, there will be a distribution of PdAu ensembles. With the previous conclusions that on close-packed PdAu surfaces all PdAu ensembles can be classified as three different 3-fold triatomic ensembles ($Au_1Pd_2$, $Au_2Pd_1$, and $Pd_3$), we consider only the three surfaces shown in Figure 1 as models in this study. Since the $Pd_{ML}(111)$ model has a $\log(r_{C-C})$ value lower than 0 when the temperature is lower than 800 K, it is expected that a pure Pd ML surface should be less catalytically active experimentally. Therefore, our theoretical modeling predicts that a PdAu surface containing Pd−Au interface sites should facilitate significant CO and $CH_4$ production, while surfaces containing only Pd(111)-like sites should be significantly less active for EtOH decomposition below 500 K. It should be noted that this kinetic model is not expected to be quantitatively accurate and only qualitative trends should be compared to experiments.[17] Therefore, in the UHV experiments discussed in the following section, we focus on mechanistic differences between the Pd−Au interface and Pd(111)-like sites under the same experimental conditions. To better understand the activity differences of the three surfaces, a d-band center model clearly shows that there is a trade-off between C−C bond cleavage and $H_2$ association: shifting the d-band toward the Fermi level leads to a lower C−C cleavage barrier but also a higher $H_2$ association barrier (Figure 5b). Thus, from a catalyst design perspective, there is no way to lower both of these barriers. This could, however, explain why $Pd_2Au_1(111)$ theoretically performs better than $Pd_1Au_2(111)$ and $Pd_{ML}(111)$: a careful tuning of the d-band center would maintain both C−C bond cleavage activity as well as $H_2$ desorption.

In addition to the kinetics and thermodynamics of the reactions, carbon coking is another important issue that should be considered. With the assumption that carbon coking correlates with the carbon binding energy through a scaling relationship, we calculated the carbon binding energy on the three modeled surfaces (Figure 6). It can be clearly seen that, with the increase of surface Pd, the carbon binding energy increases linearly, indicating that larger Pd ensembles should lead to more coking, in agreement with the d-band theory (Figure 6, inset).[39] This is consistent with our previous studies

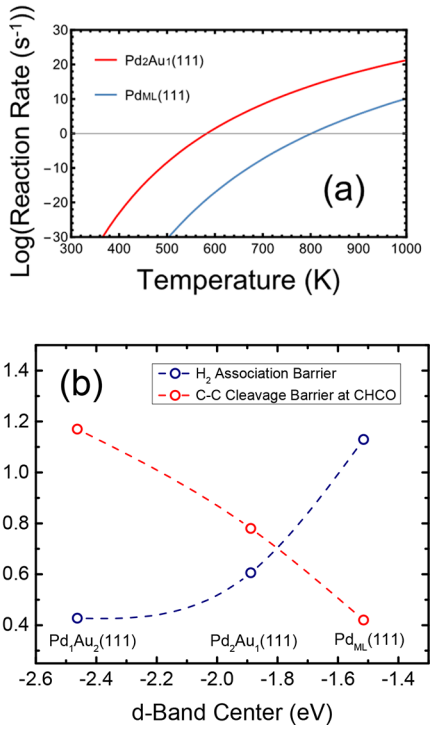


**Figure 5.** (a) Modeled reaction rates of EtOH C−C bond cleavage ($\log(r_{C-C})$, unit: $\log(s^{-1})$) on $Pd_2Au_1(111)$ and $Pd_{ML}(111)$. The catalytic modeling details can be found in the Supporting Information. (b) Calculated d-band center versus activation energies for $H_2$ association and C−C bond cleavage at CHCO.

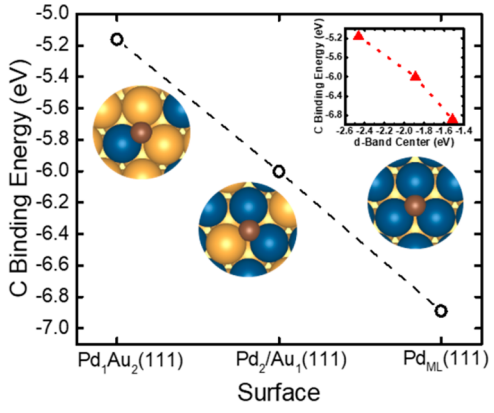


**Figure 6.** Calculated carbon binding energies on $Pd_1Au_2(111)$, $Pd_2Au_1(111)$, and $Pd_{ML}(111)$. Insets show the binding configurations. Blue, golden, and brown spheres represent Pd, Au, and C, respectively. The inset figure shows the correlation between C binding energy and the surface d-band center.



DOI: 10.1021/acs.jpcc.8b08150
J. Phys. Chem. C 2018, 122, 22024−22032

of sulfur poisoning on PdAu, where larger Pd ensembles increase sulfur poisoning on PdAu(111) and significantly decrease the nitrite reduction activity of pure Pd nanoparticles to almost zero.[28] With the calculated surface d-band, we expect the binding of other carbon species would also be strengthened when the surface Pd composition is increased, leading to significant coking. Therefore, it is expected that on the $Pd_{ML}(111)$ surface there should be less activity than $Pd_2Au_1(111)$ because of the slow $H_2$ evolution kinetics as well as additional carbon coking.

**3.3. UHV Experiments.** To provide experimental evidence for the theoretical calculations presented above, we conducted UHV experiments on Pd−Au model catalysts. In this study, we studied two Pd−Au model catalysts: Au(111) with 2 and 4 ML Pd as measured by the initial coverage. After annealing at 500 K for 10 min, the 2 ML Pd−Au coverage formed a surface containing a 74.9% Pd−Au interface and 25.1% Pd(111)-like sites, whereas the 4 ML Pd−Au coverage formed a surface containing only Pd(111)-like sites. The site composition was quantified by $H_2$ temperature-programmed desorption (TPD). Determination of the surface composition is supported by our previous studies using $H_2$, $O_2$, and CO TPD and reflection−absorption infrared spectroscopy (RAIRS) experiments for similar Pd deposition and annealing conditions.[11,12,40−44] In our previous work, we showed that the 2 ML Pd−Au catalyst showed the highest activity for $H_2$ production from EtOH at 500 K.[12] To investigate the EtOH decomposition products on the surface, we impinged 1.0 ML of EtOH (or $CD_3CH_2OH$) on 2 ML Pd−Au via a molecular beam and conducted TPD experiments, as shown in Figure 7a. Here, we see the production of CO ($m/z$ = 28) at 455 K, $CH_4$ ($m/z$ = 16) at 300 K, and HD ($m/z$ = 3) at 350 K. The production of CO and $CH_4$ is indicative of C−C bond breakage, which is consistent with previous studies on a Pd(111) surface and the theoretical work described above.[17,45] Furthermore, the HD production suggests dehydrogenation of the methyl group, making C−C bond breakage more favorable per the theoretical results shown in Figure 3. CO, $CH_4$, and $H_2$ were also produced on the 4 ML Pd−Au catalyst (not shown) at similar product yields as the 2 ML Pd−Au catalyst. This is not surprising considering that EtOH decomposition has previously been shown on Pd(111) model catalysts.[46] It is worth noting that, due to a signal contribution of background $H_2$, it was difficult to distinguish between $H_2$ that adsorbed on the surface and $H_2$ that was produced from EtOH. Therefore, we used $CD_3CH_2OH$ to highlight the decomposition of the EtOH's methyl group on the surface.

We also conducted Auger electron spectroscopy (AES) on the 2 and 4 ML Pd−Au surfaces before and after EtOH exposure (Figure 7b). There was no observation of an oxygen feature (503 eV), which we would expect if there was significant C−O cleavage of EtOH. However, we do suspect a carbon contribution to the Auger spectra on the 2 ML Pd−Au surface after EtOH desorption. Pd has three prominent features at 243, 279, and 330 eV. The 279 eV feature dwarfs the 272 eV carbon feature, making it difficult to confirm the presence of carbon on Pd surfaces. However, we see two telling changes in the second Pd feature after EtOH desorption. First, the bottom peak shifted to a lower kinetic energy by 4 to 274 eV, which suggests a convolution of the 272 eV carbon feature with the 279 eV Pd feature. Second, the peak-to-peak intensity of this feature is larger relative to the other two Pd features when compared to the clean 2 ML Pd−Au catalyst. This is

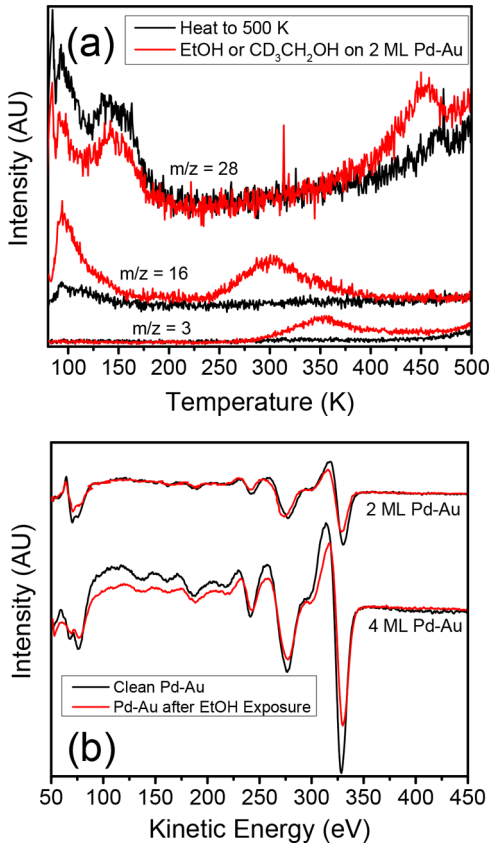


**Figure 7.** (a) TPD of 1.0 ML of EtOH on 2 ML Pd−Au catalyst at 77 K. $CD_3CH_2OH$ was used to showcase the methyl group decomposition through HD formation. (b) AES of 2 and 4 ML Pd−Au surfaces before and after TPD of 1.0 ML of EtOH.

indicative of contribution from another element, which would be carbon. Additionally, the HD production from $CD_3CH_2OH$ decomposition, shown in Figure 7a, supports the production of carbon. Dehydrogenation of the methyl group can result in surface carbon that may be observed in AES (Figure 7b). For the 4 ML Pd−Au catalyst, the 279 eV Pd feature is too large to see the presence of carbon. There is no shift in the peak nor is there a change in the relative size of this second feature. However, we suspect that there is still carbon contamination that is occurring on our catalysts, as seen on Pd(111).[46] More importantly, there was no presence of oxygen, indicating no C−O dissociation on the 4 ML Pd−Au surface. From AES, we see changes in the spectra indicative of carbon contamination from EtOH decomposition, but the absence of an oxygen feature suggests there is minimal C−O cleavage of the EtOH molecule, in agreement with the theoretical results.

Additionally, we conducted ethanol reflection−absorption infrared spectroscopy (EtOH-RAIRS) on the 2 ML Pd−Au surface to obtain insight into EtOH decomposition on the catalytic surface. In Figure 8, we have EtOH-RAIRS spectra of the 2 ML Pd−Au surface with EtOH coverages from 1 to 4 ML with the assignment of the peaks to their vibrational modes in Table 2. Assignments were made by comparison with high resolution electron energy loss (HREEL) spectroscopy of EtOH on Pd(111) and EtOH in an argon matrix.[45] At 1 ML EtOH, we see the O—H, $CH_3$, and asymmetric C—C—O stretches. Even at low coverage, the asymmetric C—C—O stretch has a relatively large intensity which is indicative of being a prominent species on the surface and is predominantly


DOI: 10.1021/acs.jpcc.8b08150
J. Phys. Chem. C 2018, 122, 22024−22032

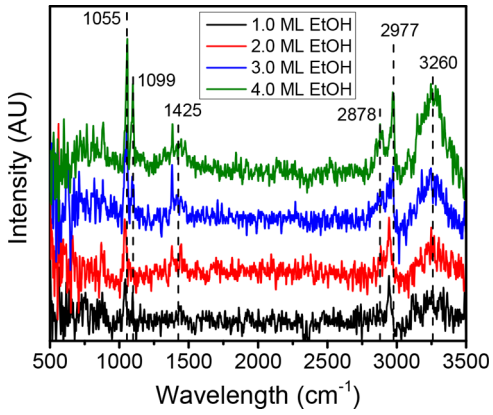


**Figure 8.** RAIRS of EtOH at different coverages on 2 ML Pd−Au at 77 K.

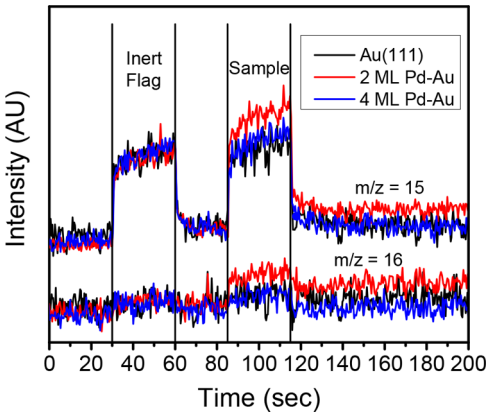


**Figure 9.** $m/z$ = 15 and 16 (methane) spectra of a modified King and Wells experiment in which EtOH was impinged on the Au(111), 2 ML Pd−Au, and 4 ML Pd−Au at 350 K.

**Table 2. Vibrational Modes and Corresponding Frequencies from EtOH-RAIRS**

| vibrational mode | frequency ($cm^{-1}$) |
|---|---|
| O−H stretch | 3260 |
| $CH_3$ stretch | 2977 |
| $CH_2$ stretch | 2878 |
| $CH_3$ and $CH_2$ deformation | 1425 |
| $CH_3$ rocking | 1099 |
| C−C−O stretch | 1055 |
| symmetric C−C−O stretch | 873 |

the stretch from the C—O bond. Therefore, C—O bond breakage is not likely to be prevalent on our surfaces. These features grow with EtOH coverage, and the peaks representative of a $CH_2$ stretch, $CH_3$ and $CH_2$ deformations, and $CH_3$ rocking appear. Conducting EtOH-RAIRS with a higher Pd coverage did not significantly change the spectra. Most importantly, there was no observation of the C═C peak from 1620 to 1680 $cm^{-1}$, which is indicative of ethylene formation and C—O bond breakage. In addition to the TPD and AES, EtOH-RAIRS builds our confidence that the C—C bond is breaking readily compared to the C—O bond, which does not show any evidence of dissociation.

In Figure 5, we describe two kinetic models that incorporate the Pd−Au interface and Pd(111)-like sites. These two models can be likened to the experiments where the 2 ML Pd−Au catalyst is representative of a hybrid of the $Pd_2Au_1(111)$ and $Pd_{ML}(111)$ models and the 4 ML Pd−Au catalyst is analogous to $Pd_{ML}(111)$. From impinging EtOH on our catalytic surfaces at elevated temperatures and detecting $CH_4$, we can provide experimental support to the theoretical reaction rates shown in Figures 5 and 6. In our previous work, we impinged EtOH on Pd−Au surfaces at 500 K, observing $H_2$ and CO evolution, but we were unable to observe a measurable amount of $CH_4$.[12] TPD of EtOH on 2 ML Pd−Au shows us that decomposition of the methyl group occurs at 350 K, as shown in Figure 7a. Therefore, impinging EtOH on the catalytic surface above 350 K results in methyl decomposition instead of methane evolution that is observable via the QMS. Lowering the temperature enables the recombination of methyl groups with H adatoms to produce methane. In Figure 9, we show methane ($m/z$ = 15 and 16) spectra from a modified King and Wells experiment[12] impinging EtOH on an inert flag followed by impingement on Au(111), 2 ML Pd−Au, or 4 ML Pd−Au at 350 K for 30 s each. EtOH is nonreactive on Au(111) at 350 K, so it can serve as a baseline for methane production compared to the other two Pd−Au surfaces. From 85 to 115 s, we see production of methane on the 2 ML Pd−Au surface, but the 4 ML Pd−Au surface resembles that of the inert Au(111) sample, which is consistent with the higher theoretical reaction rates of C−C bond breakage for the $Pd_2Au_1(111)$ surface. With the surface largely covered by Pd on the 4 ML Pd−Au catalyst, the surface remains reactive but may result in more carbon contamination instead of methane evolution. With the presence of more Au on the surface, $CH_4$ more readily desorbs, as shown by the 2 ML Pd−Au catalyst. It is worth noting that $m/z$ = 15 is also a mass fragment of EtOH, which is why there is an increase in that signal upon impinging EtOH on the inert flag. With the modified King and Wells experiment, we can further confirm C−C bond cleavage on the Pd−Au catalysts and observe better product evolution from the surface with predominately Pd−Au interface sites. These results are in good agreement with our calculations. However, given the intrinsic differences between the theoretical model[17] and the experiments, we have not compared the precise reaction temperature between theory and experiment. We also expect that a full kinetic model with more calculations of EtOH dehydrogenation mechanisms would provide a more quantitative comparison with experiment but not alter the qualitative trends derived from our present model.

## 4. CONCLUSION

In this paper, we have conducted a combined theoretical and experimental study to understand EtOH decomposition on Pd−Au alloy catalysts. Using DFT calculations and the BEP relationships, we constructed an activation energy database for possible EtOH C−C and C−O bond cleavage mechanisms on three characteristic Pd−Au close-packed surfaces: $Pd_1Au_2(111)$, $Pd_2Au_1(111)$, and $Pd_{ML}(111)$. Both the calculated kinetic and thermodynamic results show that, on PdAu(111), C−C bond cleavage is more favorable than C−O bond cleavage. Using the computational method developed from previous studies, we estimated the theoretical catalytic activities of C−C bond cleavage as a function of reaction temperature. Our results show that a $Pd_2Au_1(111)$ surface should have a high EtOH decomposition activity, while $Pd_1Au_2(111)$ and $Pd_{ML}(111)$ are less active. These results can be explained by the trade-off between C−C cleavage and $H_2$ association as a function of the surface d-band. Using UHV


DOI: 10.1021/acs.jpcc.8b08150
J. Phys. Chem. C 2018, 122, 22024−22032

EtOH decomposition experiments, we have been able to provide experimental support to the theoretical calculations. TPD of EtOH on Pd−Au shows the production of $CH_4$, CO, and $H_2$, indicating that C−C bond cleavage is favorable. The absence of oxygen in AES after EtOH decomposition and the intense peak for C−O vibration in EtOH-RAIRS suggest that C−O bond cleavage is not prominent on the Pd−Au surface. Finally, we see a similar trend in the C−C bond cleavage reaction rate where a surface containing predominantly Pd−Au interface ensembles has a higher EtOH decomposition catalytic activity than surfaces with Pd(111)-like and pure Au(111) sites. These experimental results are qualitatively consistent with the theoretical model. We expect that both the theory and experiments in this study will help to understand the activity and selectivity of EtOH decomposition on the alloyed catalytic surface and more generally for tailoring alloyed systems for industrial catalyst design.

## ■ ASSOCIATED CONTENT

### Supporting Information

The Supporting Information is available free of charge on the ACS Publications website at DOI: 10.1021/acs.jpcc.8b08150.

Modeling details, convergence tests, calculated thermodynamic and kinetic data, C−O and C−C cleavage mechanisms of CHCO, and the most significant geometric coordinates of our models (PDF)

## ■ AUTHOR INFORMATION


### Corresponding Authors

*E-mail: mullins@che.utexas.edu.
*E-mail: henkelman@utexas.edu.

### ORCID

C. Buddie Mullins: 0000-0003-1030-4801
Graeme Henkelman: 0000-0002-0336-7153


### Author Contributions

§H.L., E.J.E.: These authors contributed equally.

### Notes

The authors declare no competing financial interest.

## ■ ACKNOWLEDGMENTS

This work was funded by the Department of Energy under Contracts DE-SC0010576 (G.H.) and DE-SC0018116 (C.B.M.). Sustained support from the Welch foundation under Grant Nos. F-1841 (G.H.) and F-1436 (C.B.M.) is greatly appreciated. Computational resources were provided by the Texas Advanced Computing Center and the National Energy Research Scientific Computing Center. We would like to thank Dr. Wen-Yueh Yu for his guidance and tutelage in conducting RAIRS experiments.

## ■ REFERENCES


(1) Luo, L.; Duan, Z.; Li, H.; Kim, J.; Henkelman, G.; Crooks, R. M. Tunability of the Adsorbate Binding on Bimetallic Alloy Nanoparticles for the Optimization of Catalytic Hydrogenation. *J. Am. Chem. Soc.* **2017**, *139*, 5538−5546.

(2) Zhang, L.; Henkelman, G. Computational Design of Alloy-Core@shell Metal Nanoparticle Catalysts. *ACS Catal.* **2015**, *5* (2), 655−660.

(3) Greeley, J.; Stephens, I. E. L.; Bondarenko, a S.; Johansson, T. P.; Hansen, H. a; Jaramillo, T. F.; Rossmeisl, J.; Chorkendorff, I.; Nørskov, J. K. Alloys of Platinum and Early Transition Metals as Oxygen Reduction Electrocatalysts. *Nat. Chem.* **2009**, *1* (7), 552−556.

(4) Li, H.; Luo, L.; Kunal, P.; Bonifacio, C. S.; Duan, Z.; Yang, J. C.; Humphrey, S. M.; Crooks, R. M.; Henkelman, G. Oxygen Reduction Reaction on Classically Immiscible Bimetallics: A Case Study of RhAu. *J. Phys. Chem. C* **2018**, *122* (5), 2712−2716.

(5) Greeley, J.; Jaramillo, T. F.; Bonde, J.; Chorkendorff, I. B.; Nørskov, J. K. Computational High-Throughput Screening of Electrocatalytic Materials for Hydrogen Evolution. *Nat. Mater.* **2006**, *5* (11), 909−913.

(6) Zhang, L.; Kim, H. Y.; Henkelman, G. CO Oxidation at the Au-Cu Interface of Bimetallic Nanoclusters Supported on CeO2(111). *J. Phys. Chem. Lett.* **2013**, *4* (17), 2943−2947.

(7) García, S.; Zhang, L.; Piburn, G. W.; Henkelman, G.; Humphrey, S. M. Microwave Synthesis of Classically Immiscible Rhodium-Silver and Rhodium-Gold Alloy Nanoparticles: Highly Active Hydrogenation Catalysts. *ACS Nano* **2014**, *8* (11), 11512−11521.

(8) Piburn, G. W.; Li, H.; Kunal, P.; Henkelman, G.; Humphrey, S. M. Rapid Synthesis of Rhodium−Palladium Alloy Nanocatalysts. *ChemCatChem* **2018**, *10* (1), 329−333.

(9) Kunal, P.; Li, H.; Dewing, B. L.; Zhang, L.; Jarvis, K.; Henkelman, G.; Humphrey, S. M. Microwave-Assisted Synthesis of PdxAu100-x Alloy Nanoparticles: A Combined Experimental and Theoretical Assessment of Synthetic and Compositional Effects upon Catalytic Reactivity. *ACS Catal.* **2016**, *6* (8), 4882−4893.

(10) Li, H.; Henkelman, G. Dehydrogenation Selectivity of Ethanol on Close-Packed Transition Metal Surfaces: A Computational Study of Monometallic, Pd/Au, and Rh/Au Catalysts. *J. Phys. Chem. C* **2017**, *121* (49), 27504−27510.

(11) Yu, W. Y.; Mullen, G. M.; Flaherty, D. W.; Mullins, C. B. Selective Hydrogen Production from Formic Acid Decomposition on Pd-Au Bimetallic Surfaces. *J. Am. Chem. Soc.* **2014**, *136* (31), 11070−11078.

(12) Evans, E. J.; Li, H.; Yu, W. Y.; Mullen, G. M.; Henkelman, G.; Mullins, C. B. Mechanistic Insights on Ethanol Dehydrogenation on Pd-Au Model Catalysts: A Combined Experimental and DFT Study. *Phys. Chem. Chem. Phys.* **2017**, *19* (45), 30578−30589.

(13) Liu, P.; Nørskov, J. K. Ligand and Ensemble Effects in Adsorption on Alloy Surfaces. *Phys. Chem. Chem. Phys.* **2001**, *3* (17), 3814−3818.

(14) Zanchet, D.; Santos, J. B. O.; Damyanova, S.; Gallo, J. M. R.; Bueno, J. M. C. Toward Understanding Metal-Catalyzed Ethanol Reforming. *ACS Catal.* **2015**, *5*, 3841−3863.

(15) Williams, R. M.; Pang, S. H.; Medlin, J. W. O-H versus C-H Bond Scission Sequence in Ethanol Decomposition on Pd(111). *Surf. Sci.* **2014**, *619*, 114−118.

(16) Alcalá, R.; Mavrikakis, M.; Dumesic, J. A. DFT Studies for Cleavage of C-C and C-O Bonds in Surface Species Derived from Ethanol on Pt(111). *J. Catal.* **2003**, *218* (1), 178−190.

(17) Ferrin, P.; Simonetti, D.; Kandoi, S.; Kunkes, E.; Dumesic, J. A.; Nørskov, J. K.; Mavrikakis, M. Modeling Ethanol Decomposition on Transition Metals: A Combined Application of Scaling and Brønsted-Evans-Polanyi Relations. *J. Am. Chem. Soc.* **2009**, *131* (16), 5809−5815.

(18) Li, M.; Guo, W.; Jiangs, R.; Zhao, L.; Shan, H. Decomposition of Ethanol on Pd(111): A Density Functional Theory Stutdy. *Langmuir* **2010**, *26* (3), 1879−1888.

(19) Sutton, J. E.; Panagiotopoulou, P.; Verykios, X. E.; Vlachos, D. G. Combined DFT, Microkinetic, and Experimental Study of Ethanol Steam Reforming on Pt. *J. Phys. Chem. C* **2013**, *117* (9), 4691−4706.

(20) Choi, Y.; Liu, P. Understanding of Ethanol Decomposition on Rh(111) from Density Functional Theory and Kinetic Monte Carlo Simulations. *Catal. Today* **2011**, *165* (1), 64−70.

(21) Zhang, J.; Cao, X. M.; Hu, P.; Zhong, Z.; Borgna, A.; Wu, P. Density Functional Theory Studies of Ethanol Decomposition on Rh(211). *J. Phys. Chem. C* **2011**, *115* (45), 22429−22437.

(22) Gursahani, K. I.; Alcalá, R.; Cortright, R. D.; Dumesic, J. A. Reaction Kinetics Measurements and Analysis of Reaction Pathways




DOI: 10.1021/acs.jpcc.8b08150
J. Phys. Chem. C 2018, 122, 22024−22032

for Conversions of Acetic Acid, Ethanol, and Ethyl Acetate over Silica-Supported Pt. *Appl. Catal., A* **2001**, *222* (1−2), 369−392.
(23) Weststrate, C. J.; Gericke, H. J.; Verhoeven, M. W. G. M.; Ciobîcă, I. M.; Saib, A. M.; Niemantsverdriet, J. W. Ethanol Decomposition on Co(0001): C-O Bond Scission on a Close-Packed Cobalt Surface. *J. Phys. Chem. Lett.* **2010**, *1* (12), 1767−1770.
(24) Xu, Z. F.; Wang, Y. Effects of Alloyed Metal on the Catalysis Activity of Pt for Ethanol Partial Oxidation: Adsorption and Dehydrogenation on Pt3M (M = Pt, Ru, Sn, Re, Rh, and Pd). *J. Phys. Chem. C* **2011**, *115* (42), 20565−20571.
(25) Xu, Z.; Wang, Y. Understanding Electrocatalytic Activity Enhancement of Bimetallic Particles to Ethanol Electro-Oxidation: Ethanol Adsorption and Decomposition on PtnM (N = 6 and 9; M = Pt, Ru, and Sn). *ACS Symp. Ser.* **2013**, *1133*, 135−151.
(26) Kumar, A.; Ashok, A.; Bhosale, R. R.; Saleh, M. A. H.; Almomani, F. A.; Al-Marri, M.; Khader, M. M.; Tarlochan, F. In Situ DRIFTS Studies on Cu, Ni and CuNi Catalysts for Ethanol Decomposition Reaction. *Catal. Lett.* **2016**, *146* (4), 778−787.
(27) Skoplyak, O.; Barteau, M. A.; Chen, J. G. Comparison of H2 Production from Ethanol and Ethylene Glycol on M/Pt(1 1 1) (M = Ni, Fe, Ti) Bimetallic Surfaces. *Catal. Today* **2009**, *147* (2), 150−157.
(28) Seraj, S.; Kunal, P.; Li, H.; Henkelman, G.; Humphrey, S. M.; Werth, C. J. PdAu Alloy Nanoparticle Catalysts: Effective Candidates for Nitrite Reduction in Water. *ACS Catal.* **2017**, *7* (5), 3268−3276.
(29) Yuan, D. W.; Liu, Z. R. Atomic Ensemble Effects on Formic Acid Oxidation on PdAu Electrode Studied by First-Principles Calculations. *J. Power Sources* **2013**, *224*, 241−249.
(30) Czelej, K.; Cwieka, K.; Colmenares, J. C.; Kurzydlowski, K. J.; Xu, Y.-J. Toward a Comprehensive Understanding of Enhanced Photocatalytic Activity of the Bimetallic PdAu/TiO2 Catalyst for Selective Oxidation of Methanol to Methyl Formate. *ACS Appl. Mater. Interfaces* **2017**, *9* (37), 31825−31833.
(31) Blöchl, P. E. Projector Augmented-Wave Method. *Phys. Rev. B: Condens. Matter Mater. Phys.* **1994**, *50* (24), 17953−17979.
(32) Perdew, J. P.; Burke, K.; Ernzerhof, M. Generalized Gradient Approximation Made Simple. *Phys. Rev. Lett.* **1996**, *77* (18), 3865−3868.
(33) Pople, J. A.; Gill, P. M. W.; Johnson, B. G. Kohn—Sham Density-Functional Theory within a Finite Basis Set. *Chem. Phys. Lett.* **1992**, *199* (6), 557−560.
(34) Henkelman, G.; Uberuaga, B. P.; Jónsson, H.; Henkelman, G. A Climbing Image Nudged Elastic Band Method for Finding Saddle Points and Minimum Energy Paths. *J. Chem. Phys.* **2000**, *113* (22), 9901−9904.
(35) Zhong, W.; Liu, Y.; Zhang, D. Theoretical Study of Methanol Oxidation on the PtAu(111) Bimetallic Surface: CO Pathway vs Non-CO Pathway. *J. Phys. Chem. C* **2012**, *116* (4), 2994−3000.
(36) Wheeler, M. C.; Seets, D. C.; Mullins, C. B. Kinetics and Dynamics of the Initial Dissociative Chemisorption of Oxygen on Ru(001). *J. Chem. Phys.* **1996**, *105* (4), 1572−1583.
(37) Ferguson, B. A.; Reeves, C. T.; Mullins, C. B. Oxygen Adsorption on Si(100)2 × 1 Via Trapping-Mediated and Direct Mechanisms. *J. Chem. Phys.* **1999**, *110*, 11574−11584.
(38) Wang, J. H.; Lee, C. S.; Lin, M. C. Mechanism of Ethanol Reforming: Theoretical Foundations. *J. Phys. Chem. C* **2009**, *113* (16), 6681−6688.
(39) Hammer, B.; Nørskov, J. K. Electronic Factors Determining the Reactivity of Metal Surfaces. *Surf. Sci.* **1995**, *343* (3), 211−220.
(40) Yu, W.-Y.; Zhang, L.; Mullen, G. M.; Henkelman, G.; Mullins, C. B. Oxygen Activation and Reaction on Pd−Au Bimetallic Surfaces. *J. Phys. Chem. C* **2015**, *119* (21), 11754−11762.
(41) Yu, W.-Y.; Zhang, L.; Mullen, G. M.; Evans, E. J.; Henkelman, G.; Mullins, C. B. Effect of Annealing in Oxygen on Alloy Structures of Pd−Au Bimetallic Model Catalysts. *Phys. Chem. Chem. Phys.* **2015**, *17* (32), 20588−20596.
(42) Yu, W. Y.; Mullen, G. M.; Mullins, C. B. Interactions of Hydrogen and Carbon Monoxide on Pd-Au Bimetallic Surfaces. *J. Phys. Chem. C* **2014**, *118* (4), 2129−2137.
(43) Yu, W. Y.; Mullen, G. M.; Mullins, C. B. Hydrogen Adsorption and Absorption with Pd-Au Bimetallic Surfaces. *J. Phys. Chem. C* **2013**, *117* (38), 19535−19543.
(44) Han, S.; Mullins, C. B. Surface Alloy Composition Controlled O 2 Activation on Pd−Au Bimetallic Model Catalysts. *ACS Catal.* **2018**, *8* (4), 3641−3649.
(45) Davis, J. L.; Barteau, M. A. Spectroscopic Identification of Alkoxide, Aldehyde, and Acyl Intermediates in Alcohol Decomposition on Pd(111). *Surf. Sci.* **1990**, *235* (2−3), 235−248.
(46) Davis, J. L.; Barteau, M. A. Decarbonylation and Decomposition Pathways of Alcohol's on Pd(111). *Surf. Sci.* **1987**, *187* (2−3), 387−406.



DOI: 10.1021/acs.jpcc.8b08150
*J. Phys. Chem. C* 2018, 122, 22024−22032